ELSEVIER

Journal of Alloys and Compounds 223 (1995) 197–203

Journal of ALLOYS AND COMPOUNDS

Comparison of the electronic structure of the lanthanides and actinides

N.M. Edelstein

Chemical Sciences Division, Lawrence Berkeley Laboratory, Berkeley, CA 94720, USA

Abstract

This paper reviews the electronic structure of the 4f and 5f compounds. To this end optical and magnetic analyses of similar compounds are compared. In most cases this entails comparing trivalent actinide with trivalent lanthanide compounds although the f^1 configuration (Ce^{3+} diluted in Cs_2NaYCl_6 and Pa^{4+} diluted in Cs_2ZrCl_6) is treated in detail. In general the ground electronic states for lanthanide and actinide compounds with the same number n of f electrons (f^n) and the same coordination about the metal ions are similar, although the total crystal field splitting in the actinides is approximately twice as great as for the lanthanides. The half-filled shell f^7 is a special case with a relatively large ground state splitting in the $5f^7$ ground term caused by the effects of the much larger spin-orbit coupling.

Keywords: Electronic structure; Actinides; Lanthanides; Crystal field; Optical spectra

1. Introduction

The lanthanide series consists of the fourteen elements following lanthanum in the periodic table and is formed by the successive addition of a 4f electron to the electronic configuration of lanthanum. Because the 4f shell is an inner shell, the chemistry of the lanthanide ions are in general very similar. Although the chemical properties of the early actinide ions are quite different from those of the later actinide ions and the lanthanide series, the actinide series, in analogy with the lanthanide series, is defined as the fourteen elements following actinium in the periodic table.

The 4f orbitals in the lanthanide series are inner orbitals and do not participate in chemical bonding. In the early actinides the 5f orbitals are more extended and very close in energy to the 6d orbitals. As the atomic number increases, the 5f orbitals become more localized and progressively lower in energy relative to the 6d configuration. The relative energies of the d orbitals (5d for the lanthanides and 6d for the actinides) relative to the f configuration for the trivalent ions are shown in Fig. 1. The data are taken from Brewer [1]. It is instructive to plot the mean radius $\langle r \rangle$ of the lanthanide and actinide ions as a function of atomic number (Fig. 2). Here the mean radius is defined as follows:

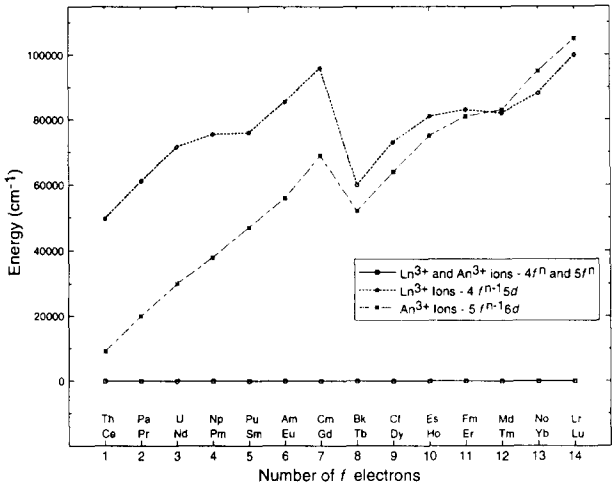

Fig. 1. Relative energies of the $f^{(n-1)}d$ configuration compared with the energies of the f^n configuration for the trivalent ions of the lanthanides and actinides, data from Ref. [1].

$$\langle r^k \rangle = \int_0^\infty P_{nl}^*(r) r^k P_{nl}(r)\, dr$$

where $P_{nl}(r)$ is the radial wavefunction with principal quantum number n, angular momentum quantum number l, and $k=1$ [2]. All quantities are in atomic units.

Ionic radii for the lanthanide and actinide ions [3] are also plotted in Fig. 2. Note the mean radii are

SSDI 0925-8388(94)09003-3

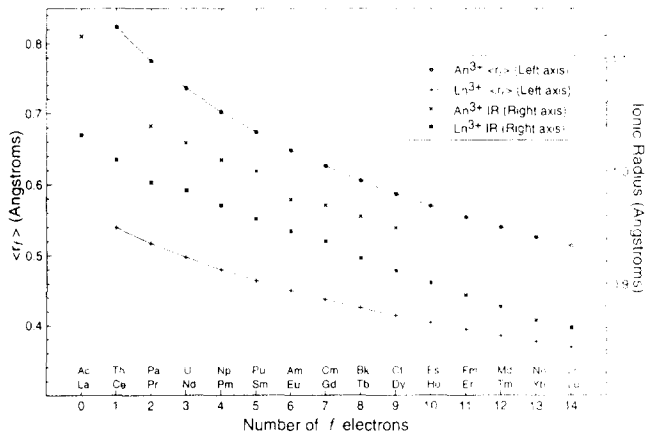

Fig. 2. Plot of the calculated mean radii $\langle r_f \rangle$ of the trivalent ions (f^n where $n=1$ to 14) of the lanthanides and actinides, and of the experimental ionic radii for these ions.

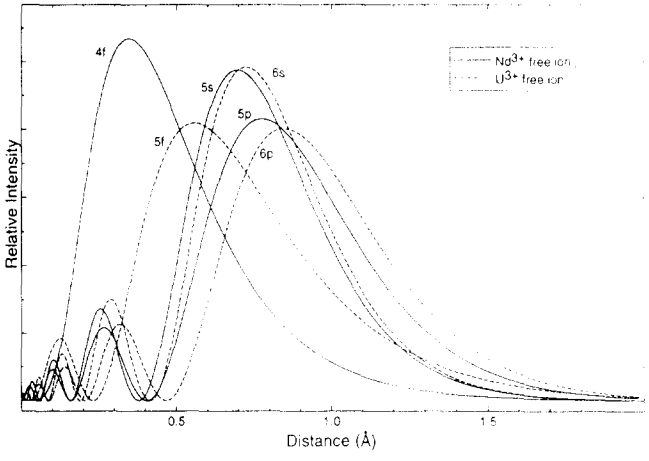

Fig. 3. Plot of the 4f, 5s, and 5p wavefunctions of Nd^{3+}, and the 5f, 6s, and 6p wavefunctions of U^{3+}.

consistently larger for the actinide series than for the lanthanides although the ionic radii for the two series are much closer to one another. This is because the ionic radii are determined not only by the f wavefunctions but also by the closed $5s^2$, $5p^6$, ($6s^2$, $6p^6$) shells. Plots of the relevant wavefunctions for Nd^{3+} and U^{3+} are shown in Fig. 3.

For the first half of the actinide series, a large number of compounds are known with formal oxidation states ranging from 2+ to 7+ [4]. Molecular compounds of actinide ions in higher oxidation states are well known. Some examples include the AnF_6 (An≡U, Np, and Pu), the transuranium borohydrides $(An(BH_4)_4$ (An≡Np, Pu), and dimeric compounds such as $[U(OC_2H_5)_5]_2$. The lighter members of the borohydride series are polymeric (Th, Pa, and U), but the Np and Pu compounds are monomeric and their physical properties resemble those of monomeric $Zr(BH_4)_4$ much more than those of polymeric $U(BH_4)_4$. Organometallic compounds are known for both the lanthanide and actinide series. If the ligand is large enough to prevent further coordination of other ligands by its steric bulk, then monomeric molecular compounds can be formed in both series. The early tetravalent actinides form organometallic compounds rather readily, and a number of these compounds show remarkable stability. For compounds of the type $[C_8H_8]_2An$ (An≡Th, Pa, U, Np, Pu) the stability of uranocene $U[C_8H_8]_2$ has been attributed to covalent bonding between the e_{2u} orbitals of the cyclooctatetrane rings and the e_{2u} f orbital [5]. Variable energy photoelectron studies [6] as well as ab initio calculations [7] show that the 6d e_{2g} orbitals and the e_{2g} orbitals of the rings make a substantial contribution to the bonding.

The purpose of this paper is to compare the electronic structures of the 4f and 5f compounds. To this end the optical and magnetic analyses of similar compounds are compared. In most cases this will entail comparing trivalent actinide with trivalent lanthanide compounds except for the f^1 configuration. First of all the standard parametric theory used in the analysis of optical and magnetic data for f^n ions is reviewed.

2. Parametric theory [8,9]

The energy levels of an f^n ion are obtained by simultaneous diagonalization of the free-ion H_{FI} and crystal-field H_{CF} Hamiltonians:

$$H_{FI} = \sum_{k=0,2,4,6} F^k(nf, nf) f_k + \zeta_f \alpha_{so} + \alpha L(L+1) + \beta G(G_2) + \gamma(R_7) + \sum_{\substack{k=2-8 \\ k\neq 5}} T^k t_k + \sum_{k=0,2,4} M^k m_k + \sum_{k=2,4,6} P^k p_k$$

and

$$H_{CF} = \sum_{k,q} B_q^k C_q^k$$

The $F^k(nf, nf)$ and ζ_f parameters above represent the radial part of the electrostatic interaction between two f electrons, and the spin–orbit interaction respectively, while f_k and α_{so} are angular parts of these interactions. The parameters α, β, γ are associated with the two-body effective operators of the configuration interaction, and the T^k are the corresponding parameters of the three-body configuration interaction operators. The M^k parameters represent the spin–spin and spin–other orbit interactions, and the P^k parameters arise from electrostatic-spin–orbit interactions with higher configurations. The number of B_q^k parameters in the crystal-field Hamiltonian is determined by the site symmetry of the metal ion. The angular operators C_q^k are the usual Racah parameters and can be evaluated by standard techniques [10].

The parameters that have a major effect on the calculated spectra are the Slater parameters $F^k(nf, nf)$, the spin–orbit coupling constant ζ_f, and the crystal-field parameters. Assignments of the observed energy levels are made and then compared with those calculated with assumed parameters from the above Hamiltonian. New assignments are then made and the parameters adjusted by a least squares routine to obtain the best fit between experiment and calculation. The "best" fit is obtained when the value of σ (in cm^{-1}) is at a minimum where

$$\sigma=[\sum(E_{obs}-E_{calc})^2/(n-p)]^{1/2}$$

where E_{obs}, E_{calc} are the observed and calculated energies, n the number of observed levels, and p the number of parameters varied.

The wavefunctions and energy splittings determined from the above Hamiltonian can be used to calculate magnetic susceptibility as a function of temperature, magnetic dipole transition strengths, and g values for crystal-field states. Some representative values for the parameters of the Hamiltonian for some trivalent lanthanide and actinide ions in $LaCl_3$ are given in Table 1 [11,12].

For the f^1 case the Hamiltonian is considerably simplified as the only parameters in this case are the spin–orbit coupling constant and the crystal-field parameters. For the f^2 case all three-body operators are zero.

3. The f^1 ion in octahedral symmetry

The two systems, Ce^{3+}/Cs_2NaYCl_6 and Pa^{4+}/Cs_2ZrCl_6, have been thoroughly studied [13–16]. In both cases the $4f^1$ or $5f^1$ ion is surrounded by six Cl^- ions in an octahedral array. Both systems show fluorescence from the lowest level of the excited d configuration (at about 28 000 cm^{-1} for Ce^{3+} and 20 000 cm^{-1} for Pa^{4+}) to the f configuration, and the energies of four of the five expected crystal field states of the f configuration are accurately determined. These energies may be fit by diagonalizing the matrices obtained from an empirical Hamiltonian and adjusting the parameters to this Hamiltonian. In this simple case there are two crystal-field parameters and one spin–orbit coupling parameter. Since there are three energy differences and three parameters, the fit is perfect. However, the fit may be checked by calculating the ground state g values and comparing them with the experimental values. The results are shown in Table 2.

Note that for Ce^{3+}/Cs_2NaYCl_6 the agreement is excellent, but for Pa^{4+}/Cs_2ZrCl_6 the calculated g value is quite a bit off from the experimental value. This is a general result when actinide and lanthanide fits are compared, the crystal-field model (the combination of the free-ion Hamiltonian with one-body crystal-field operators) works rather well for the 4f series, but shows much greater deviations for 5f ions. Of course, Pa^{4+} is tetravalent and is subject to a considerably larger

Table 1
Energy level parameters for representative lanthanide and actinide ions diluted in $LaCl_3$, all values in cm^{-1}

Parameter	$Nd^{3+}(4f^3)$ [a]	$Er^{3+}(4f^{11})$ [a]	$U^{3+}(5f^3)$ [b]	$Fm^{3+}(5f^{11})$ [b]
F^2	71866	98203	39611	65850
F^2	52132	69647	32960	52044
F^6	35473	49087	23084	37756
ζ	880	2370	1626	4326
α	22.1	15.9	29.26	30
β	−650	−632	−824.6	−600
γ	1586	2017	1093	450
T^2	377	300	306	100
T^3	40	48	42	45
T^4	63	18	188	50
T^6	−292	−342	−242	−300
T^7	358	214	447	640
T^8	354	449	300	400
M^0	1.97	4.5	0.672	1.587
M^2	1.1	2.52	0.372	0.878
M^4	0.75	1.71	0.258	0.612
P^2	255	667	1216	600
P^4	191	500	608	300
P^6	128	334	121.6	60
B_0^2	107	216	287	306
B_0^4	−342	−271	−662	−1062
B_0^6	−677	−411	−1340	−1441
B_6^6	466	272	1070	941

[a] From Ref. [11].
[b] From Ref. [12].

Table 2
Experimental and calculated energy levels and ground state g values for Ce^{3+}/Cs_2NaYCl_6 and Pa^{4+}/Cs_2ZrCl_6

Crystal field levels and g value	Pa^{4+} energy levels [a] (Experimental)	Pa^{4+} energy levels [a] (Calculated)	Ce^{3+} energy levels [b] (Experimental)	Ce^{3+} energy levels [b] (Calculated)
5d or 6d (Γ_{8g}') (cm^{-1})	40000	40000[c]	>50000	50000 [d]
5d or 6d (Γ_{7g}) (cm^{-1})	23000	23000	29435	29435
5d or 6d (Γ_{8g}) (cm^{-1})	19954	19954	28196	28196
$^2F_{7/2}$ (Γ_{6u}) (cm^{-1})	8173 ± 3	8173 [e]	3085.6 ± 2	3085.6 [f]
$^2F_{7/2}$ (Γ_{8u}') (cm^{-1})	7272 ± 3	7272	2688.8 ± 2	2688.8
$^2F_{7/2}$ (Γ_{7u}') (cm^{-1})	5250 ± 50	5539	2159 ± 50	2160.1
$^2F_{5/2}$ Γ_{8u} (cm^{-1})	2108 ± 1	2108	598.5 ± 2	598.5
$^2F_{5/2}$ Γ_{7u} (cm^{-1})	0	0	0	0
$g_{\Gamma 7u}$	−1.141 ± 0.002	−0.953	−1.266	−1.255

[a] Refs. [14] and [15].
[b] Refs. [13] and [16].
[c] 10Dq = 18600 cm^{-1}, ζ_{6d} = 1856.5 cm^{-1}, E_{ave} = 28582 cm^{-1}.
[d] 10Dq = 21318 cm^{-1}, ζ_{5d} = 796.8 cm^{-1}, E_{ave} = 37165 cm^{-1}.
[e] B_0^4 = 6945.3 cm^{-1}, B_0^6 = −162.7 cm^{-1}, ζ_{5f} = 1539.6 cm^{-1}.
[f] B_0^4 = 2219.1 cm^{-1}, B_0^6 = −254.9 cm^{-1}, ζ_{4f} = 622.7 cm^{-1}.

crystal-field than Ce^{3+}. In addition the greater spatial extent of the 5f wavefunction could result in greater covalent bonding with the Cl^- ligands. As expected the spin-orbit coupling constant for the 6d configuration in Pa^{4+} is much larger than for the 5d configuration in Ce^{3+}, although it appears that 10Dq (the crystal-field splitting of one d electron in an octahedral field, defined as the difference between the energies of the e_{2g} and t_{2g} orbitals in the absence of spin-orbit coupling) is larger for Ce^{3+}/Cs_2NaYCl_6 than for Pa^{4+}/Cs_2ZrCl_6. However this latter number is uncertain and the differences in 10Dq do not appear to be significantly different.

4. Comparison of An^{3+} and Ln^{3+} in $LaCl_3$

Carnall [11] has recently published a compendium of the data for $An^{3+}/LaCl_3$ and his analysis of these data. He carried out a new energy level analysis for the entire series where data are available (from U^{3+} through Es^{3+}). The values of σ for the actinides (which are a measure of the quality of the fits) are between 20 and 22 cm^{-1}. This compares with values of σ for the lanthanides on the order of 10 cm^{-1}. Carnall was able to arrive at a consistent analysis by assuming the parameters of the principal interactions showed uniform trends as a function of atomic number. The exception to this trend occurred at the beginning of the series where the parameters for U^{3+} (free ion as well as crystal field) were not consistent with the data for the heavier ions. The crystal-field parameters for the actinides are approximately twice as large as those for the lanthanides, except for B_0^2 (not including U^{3+}) where the values for the lighter actinides are of the same order as those in the lanthanide series. Carnall also compared the splittings of the ground terms of each member of the lanthanide and actinide series with the same number of f electrons. For most cases the ordering of the crystal field states (labeled by the quantum number μ where $Jz = \mu(\mathrm{mod}\ q)$ [10]) is the same in both the lanthanide and actinide ions.

The total crystal-field strength has been defined by Auzel and Malta [17] as

$$N_v' = \frac{N_v}{2\pi}\left[\sum_{k,q}(B_q^k)^2/(2k+1)\right]^{1/2}$$

with N_v' in units of cm^{-1}.

A comparison of the values of N_v' for the lanthanide and actinide series is given in Fig. 4. It appears the strength of the crystal field in the actinides is about a factor of two larger than in the lanthanides. Note

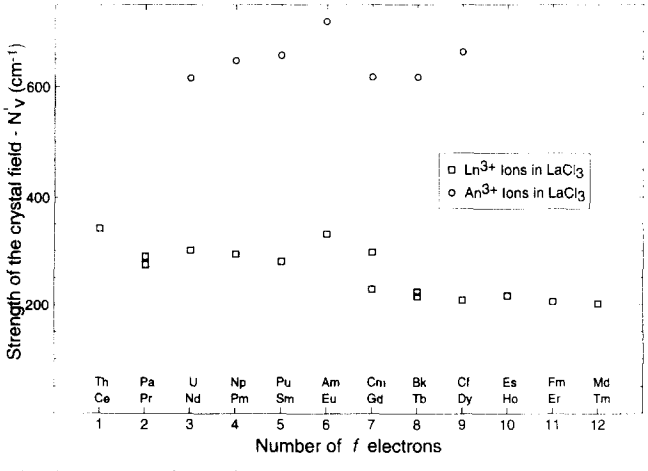

Fig. 4. A comparison of the N_v' values obtained from the crystal-field parameters for Ln^{3+} and An^{3+} in $LaCl_3$.

that in the lanthanides the crystal-field strength for the latter half of the series is less than in the first half of the series, but no trend is discernible in the actinides. Of course there are relatively sparse data for the actinides, so this generalization must be treated with caution.

5. f-Element organometallic compounds

Although actinide organometallic chemistry is a very active area of interest, only a few detailed optical or magnetic measurements have been reported on trivalent actinide organometallic compounds. For this review two sets of compounds have been chosen; $Cp_3''Th$, $Cp_3''Ce$ and $Cp_3''U \cdot L$, $Cp_3''Nd \cdot L$ where $L \equiv CNC(CH_3)_3$ and $Cp'' \equiv \eta^5-C_5H_3(SiMe_3)_2$ [18–20]. Low temperature electron paramagnetic resonance (epr) and magnetic susceptibility data measured as a function of temperature are available for this series of compounds. The data for the $Cp_3''U \cdot L$, $Cp_3''Nd \cdot L$ pair are given in Table 3. It is clear that the ground crystal-field states are similar for the Nd and U compounds. The difference between the room temperature magnetic susceptibilities can be explained by a larger crystal-field splitting in the U compound as compared with the Nd compound.

For the Th^{3+} free ion, the ground configuration is $5f^1$ with the $6d^1$ configuration at about 10 000 cm^{-1}. In compounds however the 6d configuration is stabilized with respect to the 5f configuration, and in $Cp_3''Th$ it becomes the ground configuration [18]. For the Ce^{3+} free ion, the ground configuration is $4f^1$ and the $5d^1$ excited configuration is at about 50 000 cm^{-1}. In $Cp_3''Ce$ the start of the 5d configuration is at about 17 000 cm^{-1}. Table 4 shows the epr data for $Cp_3''Ce$, $Cp_3''Th$, Cp_3Zr and $(MeCp)_3Zr$ ($Cp \equiv \eta^5-C_5H_5$, $MeCp \equiv \eta^5-C_5H_4CH_3$) [19,20]. Clearly the g values for the ground state of $ThCp_3''$ match those of Cp_3Zr and $(MeCp)_3Zr$ much more closely than those of $Cp_3''Ce$ which verifies the assignment of the ground state in the Th compounds as the d_{z^2} orbital.

6. Comparison of Eu^{3+}/ThO_2 and Am^{3+}/ThO_2

Optical spectra for Eu^{3+}/ThO_2 and Am^{3+}/ThO_2 have recently been reported [21] and provide another host matrix in which to compare the effects of the crystal field on the f^6 configuration. Table 5 shows the values of the parameters found from the analysis. The larger crystal field found for the actinides and especially for the ThO_2 matrix causes extensive J mixing in Am^{3+}. This is in contrast to Eu^{3+} where the states show rather pure L–S coupling. Again the values of the parameter N_v' show that the total crystal field strength in Am^{3+}/ThO_2 is 2.4 times greater than that in Eu^{3+}/ThO_2.

7. The f^7 configuration

The ground state wavefunction of Gd^{3+} ($4f^7$) is an almost pure $^8S_{7/2}$ state which, because $L=0$, should undergo no splitting in a crystalline field. However, for this ion and ions of the d transition metals, small splittings are observed. Much work has been done on various higher-order interactions which can cause these splittings but the mechanisms are still not well understood. For the Gd^{3+} ion in various hosts, the extent of the ground state splittings is on the order of 0.5 cm^{-1} or less. For Cm^{3+} in various host crystals the ground state splittings are on the order of 10 cm^{-1} [21]. Some data from epr measurements on Cm^{3+} in various crystals compared with Gd^{3+} are shown in Table 6 [23]. The reason for the rather large differences in the splittings of the ground term between Gd^{3+} and Cm^{3+} can be explained by the large spin–orbit coupling in Cm^{3+}. Table 7 shows the free-ion wavefunctions for Gd^{3+} and Cm^{3+}. The Cm^{3+} free-ion wavefunction consists of 50 L–S terms of which those with $L>1$ can split in a crystal field. It has been shown that by adding up all these terms the calculated splittings found for Cm^{3+} agree quite well with the measured values. This is not true for Gd^{3+}, as a large number of interactions of approximately the same magnitude contribute to the observed splittings.

Sytsma et al. [24] have recently completed an analysis of the optical spectra of Gd^{3+} and Cm^{3+} in the tetragonal host crystal $LuPO_4$. Earlier work on the epr of $Cm^{3+}/LuPO_4$ had been analyzed in terms of a total ground term splitting of approximately 11 cm^{-1}. The optical analysis confirms this splitting and Sytsma et al. obtained crystal-field parameters for both Gd^{3+} and Cm^{3+} in $LuPO_4$. The parameters obtained from the

Table 3
Magnetic susceptibility and electron paramagnetic resonance data for $Cp_3''M \cdot CNC(CH_3)_3$ (M≡Nd, U), data from Ref. [20]

Compound	g_1 [a]	g_2 [a]	g_3 [a]	g_{ave}(epr) [a]	g_{ave}(susceptibility) [b]	μ_{eff}(BM) [c]
$Cp_3''Nd \cdot CNC(CH_3)_3$	2.231	2.095	0.856	1.73	1.66	3.85
$Cp_3''U \cdot CNC(CH_3)_3$	2.463	1.739	<0.7	$1.39<g<1.63$	1.69	3.13

[a] At approximately 10 K.
[b] Temperature range 5–10 K, $S'=1/2$.
[c] Temperature range 200–300 K.

Table 4
Epr data for various f^1 or d^1 organometallic compounds

	Configuration	g_{11}	$g_\perp$	g_{ave}	Temperature (K)	Reference
$Cp_3''Th$ in MCH [a]	$6d^1$			1.910 ± 0.001	300	[18]
$Cp_3''Th$ in MCH	$6d^1$	1.9725 ± 0.001	1.879 ± 0.001	1.910 [b]	10–110	[18]
$Cp_3''Th$ powder	$6d^1$	1.972 ± 0.001	1.878 ± 0.001	1.909 [b]	10–300	[18]
Cp_3Zr in 2-MeTHF [c]	$4d^1$	1.999	1.970	1.980 [b]	100	[20]
Cp_3Zr in 2-MeTHF	$4d^1$			1.977	298	[20]
$(CH_3Cp)_3Zr$ in 2-MeTHF	$4d^1$	1.999	1.969	1.979 [b]	100	[20]
$(CH_3Cp)_3Zr$ in 2-MeTHF	$4d^1$			1.977	298	[20]
$Cp_3''Ce$ powder	$4f^1$	2.77	2.39	2.52 [b]	5	[19]

[a] MCH is methylcyclohexane.
[b] Calculated from (1/3) $(g_{11} + 2g_\perp)$.
[c] 2-MeTHF is 2-methyltetrahydrofuran.

Table 5
Spectroscopic parameters for Eu^{3+} and Am^{3+} diluted in ThO_2, from Ref. [21], all values in cm^{-1}

Parameter	Eu^{3+}/ThO_2 [a]	Am^{3+}/ThO_2 [b]
F^2	[80335.2] [c]	48038.0(140.2) [d]
F^4	[58953.9]	39684.2(212.9)
F^6	[41636.6]	29514.1(171.4)
ζ	1337.3(7.1)	2511.1(27.0)
α	[16.8]	33.2(8.6)
β	[−640]	[−660]
γ	[1750]	[1000]
T^2	[370]	[200]
T^3	[40]	[50]
T^4	[40]	[40]
T^6	[−330]	[−360]
T^7	[380]	[390]
T^8	[370]	[340]
M^0	[2.38]	[0.99]
M^2	[1.33]	[0.55]
M^4	[0.90]	[0.38]
P^2	[245]	[850]
P^4	[183.8]	[637.5]
P^6	[122.5]	[425]
B_0^4	−2780.2(32.2)	−6731.3(96.0)
B_0^6	266.0(26.3)	713.6(115)
N_v'	1212	2945

[a] 17 experimental levels, rms deviation 18.0 cm^{-1}.
[b] 17 experimental levels, rms deviation 47.3 cm^{-1}.
[c] All parameter values in [] held fixed in the fitting procedure.
[d] Number in () is the standard deviation of the parameter.

Table 6
Comparison of the ground state crystal-field splittings of Gd^{3+} and Cm^{3+} in cubic crystals (Ref. [23])

Host	Lattice constant (Å)	Gd^{3+} (cm^{-1})	Cm^{3+} (cm^{-1})
CeO_2	5.41	0.0653	17.8
ThO_2	5.60	0.06645	15.5
CaF_2	5.46	0.0578	13.4
SrF_2	5.80	0.0501	11.2
$SrCl_2$	7.00	0.0198	5.13

Table 7
Free-ion wavefunctions for Gd^{3+} and Cm^{3+}, parameters from Ref. [24]

L–S term	Gd^{3+}		Cm^{3+}	
	Component	Percentage	Component	Percentage
^8S	−0.9857	97.16	0.8859	78.48
^6P	−0.1666	2.77	−0.4232	17.91
$^4D6$	−0.0146	0.0213	−0.1052	1.107
$^4D1$	−0.0144	0.0207	−0.1039	1.079
^6D	0.0127	0.0161	0.0926	0.857
$^4D4$	0.0031	0.96×10^{-3}	0.0205	42.0×10^{-3}
$^4F4$	0.0020	0.40×10^{-3}	0.0409	0.167
$^2F6$	0.0016	0.26×10^{-3}	0.0322	0.103
^6F	−0.0011	0.12×10^{-3}	−0.0227	51.5×10^{-3}
$^4D3$	−0.0011	0.12×10^{-3}	−0.0226	51.1×10^{-3}

optical analyses are shown in Table 8. Again we see that N_v' is about twice as large for Cm^{3+} as for Gd^{3+}.

8. Conclusion

The optical data available for f^n ions of the same oxidation state have been reviewed. Using the Auzel and Malta parameter N_v' as a measure of the strength of the crystal field, one finds the actinide crystal field is approximately twice that of the corresponding lanthanide ion. From an electrostatic model the crystal-field parameters B_q^k can be written as [25]

$$B_q^k = A_q^k \langle r^k \rangle$$

where the value of A_q^k depends on the type of electrostatic model assumed. Since the ionic radii of the actinide and lanthanide ions are similar, it is expected that the values of A_q^k for ions of the lanthanide and actinide series should be similar. Thus, qualitatively, one can attribute the larger crystal-field interactions in the actinide series to the more extended nature of the 5f wavefunctions as given by $\langle r^k \rangle$. However, this

Table 8
Energy level parameters for Gd^{3+} and Cm^{3+} diluted in $LuPO_4$ from Ref. [24], all values in cm^{-1}

Parameter	Gd^{3+} [a]	Cm^{3+} [b]
F^2	84075	54669
F^4	61411	44760
F^6	44426	33021
ζ	1494	2867.7
α	[18.9] [c]	30.3
β	[−600]	−982
γ	[1575]	749
T^2	[300]	[200]
T^3	[42]	[50]
T^4	[62]	[40]
T^6	[−295]	[−360]
T^7	[350]	[390]
T^8	[310]	[340]
M^0	[3.22]	[1.09]
M^2	[1.80]	[0.61]
M^4	[1.22]	[0.41]
P^2	[676]	[912]
P^4	[507]	[684]
P^6	[338]	[456]
B_0^2	168.6	442.7
B_0^4	220.1	304.1
B_4^4	−1034.2	−1980.3
B_0^6	−733.4	−2880.1
B_4^6	960.6	881.3
N_v'	657.3	1295.6

[a] 44 experimental levels, $\sigma = 15.1\ cm^{-1}$.
[b] 60 experimental levels, $\sigma = 30.8\ cm^{-1}$.
[c] Values in [] held fixed.

is a gross oversimplification as this model does not include f-orbital covalency, whose effects are clearly observed in epr experiments. For example, a large superhyperfine structure has been reported for PuF_8^{5-} (Pu^{3+} in the cubic site of CaF_2) [26]. The incorporation of covalency effects into a ligand field model and its application to the actinides needs further implementation.

Acknowledgement

This work was supported by the Director, Office of Energy Research, Office of Basic Energy Sciences, Chemical Sciences Division of the US Department of Energy under Contract No. DE-AC03-76SF00098.

References

[1] L. Brewer, *J. Opt. Soc. Am., 61* (1971) 1666.
[2] R.D. Cowan, *The Theory of Atomic Structure and Spectra,* University of California Press, Berkeley, CA, 1981, p. 72.
[3] R.D. Shannon, *Acta Crystallogr. A, 32* (1976) 751.
[4] J.J. Katz, G.T. Seaborg and L.R. Morss (eds.), *The Chemistry of the Actinide Elements,* Chapman and Hall, London, 1986.
[5] T.J. Marks and A. Streitwiser, Jr., Organoactinide chemistry: properties of compounds having metal–carbon bonds only to π-bonded ligands. In J.J. Katz, G.T. Seaborg and L.R. Morss (eds.), *The Chemistry of the Actinide Elements,* Chapman and Hall, London, 1986, Chapter 22.
[6] J.G. Brennan, J.C. Green and C.M. Redfern, *J. Am. Chem. Soc., 111* (1989) 2373.
[7] A.H. Chang and R.M. Pitzer, *J. Am. Chem. Soc., 111* (1989) 2500.
[8] H.M. Crosswhite and H. Crosswhite, *J. Opt. Soc. Am. B, 1* (1984) 246.
[9] W.T. Carnall, H. Crosswhite, H.M. Crosswhite, J.P. Hessler, N. Edelstein, J.G. Conway, G.V. Shalimoff and R. Sarup, *J. Chem. Phys., 72* (1980) 5089.
[10] B.G. Wybourne, *Spectroscopic Properties of Rare Earths,* Wiley, New York, 1965.
[11] W.T. Carnall, *J. Chem. Phys., 96* (1992) 8713.
[12] W.T. Carnall, H. Crosswhite and H.M. Crosswhite, *Special Report 1977* (Chemistry Division, Argonne National Laboratory, Argonne, IL).
[13] R.W. Schwartz and P.N. Schatz, *Phys. Rev. B, 8* (1973) 3229.
[14] D. Piehler, W.K. Kot and N. Edelstein, *J. Chem. Phys., 94* (1991) 942.
[15] N. Edelstein, W.K. Kot and J.C. Krupa, *J. Chem. Phys., 96* (1992) 1.
[16] K. Murdoch, P. Tanner and N. Edelstein, unpublished data.
[17] F. Auzel and O.L. Malta, *J. Phys., 44* (1983) 210.
[18] W.K. Kot, G.V. Shalimoff, N.M. Edelstein, M.A. Edelman and M.F. Lappert, *J. Am. Chem. Soc., 110* (1988) 986.
[19] W.K. Kot, *PhD Thesis,* LBL-30652, Lawrence Berkeley Laboratory, Berkeley, CA, 1991.
[20] W. Lukens and R.A. Andersen, unpublished data.
[21] S. Hubert, P. Thouvenot and N. Edelstein, *Phys. Rev. B, 48* (1993) 5751.
[22] W.K. Kot, N.M. Edelstein, M.M. Abraham and L.A. Boatner, *Phys. Rev. B, 48* (1993) 12704.
[23] W. Kolbe, N. Edelstein, C.B. Finch and M.M. Abraham, *J. Chem. Phys., 58* (1973) 820.
[24] J. Sytsma, N. Edelstein, M.M. Abraham and L. Boatner, unpublished data.
[25] B.C. Wybourne, *Spectroscopic Properties of Rare Earths,* Wiley, New York, 1965, pp. 213–219.
[26] W. Kolbe and N. Edelstein, *Phys. Rev. B, 4* (1971) 2869.